



Ammonia gas sensors based on $\text{In}_2\text{O}_3/\text{PANI}$ hetero-nanofibers operating at room temperature

Qingxin Nie, Zengyuan Pang, Hangyi Lu, Yibing Cai and Qufu Wei*

Full Research Paper

Open Access

Address:

Key Laboratory of Eco-Textiles, Ministry of Education, Jiangnan University, 214122 Wuxi, Jiangsu, China

Email:

Qufu Wei* - qfwei@jiangnan.edu.cn

* Corresponding author

Keywords:

ammonia (NH_3); electrospinning; gas sensor; indium(III) oxide (In_2O_3); polyaniline (PANI)

Beilstein J. Nanotechnol. **2016**, *7*, 1312–1321.

doi:10.3762/bjnano.7.122

Received: 06 April 2016

Accepted: 06 September 2016

Published: 19 September 2016

This article is part of the Thematic Series "Nanostructures for sensors, electronics, energy and environment III".

Guest Editor: N. Motta

© 2016 Nie et al.; licensee Beilstein-Institut.

License and terms: see end of document.

Abstract

Indium nitrate/polyvinyl pyrrolidone ($\text{In}(\text{NO}_3)_3/\text{PVP}$) composite nanofibers were synthesized via electrospinning, and then hollow structure indium oxide (In_2O_3) nanofibers were obtained through calcination with PVP as template material. In situ polymerization was used to prepare indium oxide/polyaniline ($\text{In}_2\text{O}_3/\text{PANI}$) composite nanofibers with different mass ratios of In_2O_3 to aniline. The structure and morphology of $\text{In}(\text{NO}_3)_3/\text{PVP}$, $\text{In}_2\text{O}_3/\text{PANI}$ composite nanofibers and pure PANI were investigated by scanning electron microscopy (SEM), Fourier transform infrared spectroscopy (FTIR), X-ray diffraction (XRD), transmission electron microscopy (TEM) and current–voltage (I – V) measurements. The gas sensing properties of these materials towards NH_3 vapor (100 to 1000 ppm) were measured at room temperature. The results revealed that the gas sensing abilities of $\text{In}_2\text{O}_3/\text{PANI}$ composite nanofibers were better than pure PANI. In addition, the mass ratio of In_2O_3 to aniline and the p–n heterostructure between In_2O_3 and PANI influences the sensing performance of the $\text{In}_2\text{O}_3/\text{PANI}$ composite nanofibers. In this paper, $\text{In}_2\text{O}_3/\text{PANI}$ composite nanofibers with a mass ratio of 1:2 exhibited the highest response values, excellent selectivity, good repeatability and reversibility.

Introduction

With the development of modern industry, environmental pollution in the form of air pollution, water pollution and soil pollution has become ever more serious [1]. With regard to this, considerable attention has been paid to air pollution. Ammonia (NH_3), as a highly toxic gas, can be emitted by natural and industrial sources and threaten human health [2–4]. NH_3 at concentrations of 50 ppm may irritate the human respiratory system, skin and eyes [4]. Higher concentrations of NH_3 will cause blindness, seizures, lung disease and even death [5–7]. So,

there is an urgent need to develop a kind of gas sensor with high sensitivity and selectivity to detect NH_3 at room temperature.

Metal oxide semiconductors can be applied as sensing materials for monitoring NH_3 . Ammonia sensors based on In_2O_3 [8], TiO_2 [9], SnO_2 [10], ZnO [11] and WO_3 [12] have been reported. Indium oxide (In_2O_3) is an n-type semiconductor with a band gap of approximately 3.55–3.75 eV, which has been widely used due to its excellent electrical and optical properties.

In_2O_3 also exhibits sensitivity to various vapors and gases, such as NO_2 [13], CO [14], H_2 [15], acetone [16] and formaldehyde [17]. However, for most metal oxides, there is the drawback of a required high operation temperature, about $300\text{ }^\circ\text{C}$, which will increase the energy consumption [18]. Compared with metal oxides, sensors based on conducting polymers show low power consumption and can be operated at room temperature. In addition, they exhibit a large specific area, small size and low weight, and they are easy to integrate with existing electronics [19,20]. Because of the environmental stability, easy synthesis and reversible doping behavior, polyaniline (PANI), as one of the most commonly used conducting polymers has received considerable attention. However, the sensitivity of PANI remains to be improved [21,22]. To conquer the limitations mentioned above, the combination of metal oxide and conducting polymers have been developed as an effective way to achieve enhanced performance [21,23-27].

In this paper, In_2O_3 /PANI composite nanofibers were prepared by the combination of electrospinning technique, calcination method and in situ polymerization. This study presents the improved response capabilities of gas sensors based on In_2O_3 /PANI composite nanofibers, which were synthesized with different ratios between In_2O_3 and aniline during the in situ polymerization. All sensors were tested at room temperature in a concentration range of NH_3 from 100 to 1000 ppm.

Experimental

Materials

Polyvinylpyrrolidone-K90 (PVP-K90, $M_w = 1.3 \times 10^6$ g/mol) was purchased from Bo Di Industrial Co. Ltd of Tianjin. Indium nitrate hydrate, *N,N*-dimethylformamide (DMF), ethyl alcohol, aniline monomer (An), ammonium persulfate (APS), hydrochloric acid (HCl, 37%), ammonium hydroxide (NH_4OH) and *m*-cresol were obtained from Sinopharm Chemical Reagent Co., Ltd. (Shanghai, China). All chemicals and reagents were used as received, except for aniline monomer. Distilled aniline monomer and deionized water were used in this study.

Preparation of hollow In_2O_3 nanofibers

The $\text{In}(\text{NO}_3)_3$ /PVP composite nanofibers were fabricated via single-nozzle electrospinning. $\text{In}(\text{NO}_3)_3 \cdot 4.5\text{H}_2\text{O}$ (1.059 g) and PVP (3.529 g) were added into 10 mL ethyl alcohol and 10 mL DMF. The mixture was stirred at $65\text{ }^\circ\text{C}$ until all the solutes were fully dissolved. The precursor solution was poured into the syringe for electrospinning. The parameters of the electrospinning were: a needle-to-collector distance of 16 cm, a voltage of 16 kV, and a feed rate of 0.5 mL/h. Then the In_2O_3 nanofibers were synthesized by annealing the precursor composite nanofibers at $800\text{ }^\circ\text{C}$ for 3 h after heating from room temperature at a rate of $0.5\text{ }^\circ\text{C}/\text{min}$.

Preparation of In_2O_3 /PANI composite nanofibers

Firstly, 0.1 g In_2O_3 nanofibers, which had been ground in an agate mortar, were added into 200 mL 1.2 mol/L HCl solution with ultrasonication treatment. Then a certain amount of aniline in HCl solution was added to the above suspension. After that, 30 mL 1.2 mol/L HCl solution containing APS was slowly dripped into the suspension to initiate the polymerization. The mass ratios of In_2O_3 nanofibers to aniline were 1:1, 1:2 and 1:4. The molar ratio of aniline to APS was 1:1. The in situ polymerization of aniline was carried out in an ice bath at $0\text{--}5\text{ }^\circ\text{C}$. The reaction lasted for 5 h. The suspension was taken out and left for 30 min, and then washed with deionized water and centrifuged for 5 min. At last, the composite nanofibers were filtered and dried in vacuum at $50\text{ }^\circ\text{C}$ for 48 h. The schematic of the preparation of In_2O_3 /PANI composite nanofibers is illustrated in Figure 1.

Fabrication of In_2O_3 /PANI gas sensors

The ground In_2O_3 /PANI nanofibers and pure PANI were mixed with *m*-cresol to form pastes, in which the weight ratio of In_2O_3 /PANI or PANI to *m*-cresol was 1:10. Each paste was coated onto interdigital electrodes to construct a sensing film and dried at $55\text{ }^\circ\text{C}$ for 2 h in air. Four thin film sensors with different mass ratios of In_2O_3 to aniline (0, 1:1, 1:2 and 1:4) were prepared. Correspondingly, the four sensors were denoted as PANI sensor, In_2O_3 /PANI-1 nanofibers sensor, In_2O_3 /PANI-2 nanofibers sensor and In_2O_3 /PANI-3 nanofibers sensor.

Structural characterization and gas sensing test

The crystal structure of In_2O_3 nanofibers was characterized by X-ray diffraction (XRD; D8, Bruker AXS, Germany) in a 2θ region of $3\text{--}90^\circ$ with $\text{Cu K}\alpha$ radiation. The morphologies and structures of the In_2O_3 nanofibers, PANI and PANI/ In_2O_3 composite nanofibers were examined by field emission scanning electron microscopy (FESEM, S-4800 and SU-1510, Hitachi, Tokyo, Japan), transmission electron microscopy (TEM; JEM-2100HR, JEOL), and Fourier transform infrared (FTIR) spectroscopy in the range of $4000\text{--}400\text{ cm}^{-1}$ with a 4 cm^{-1} spectral resolution (NEXUS 470 spectrometer, Nicolet, Madison, WI, USA). *I*-*V* measurements were carried out on a CHI 660E electrochemical workstation (CH Instruments, Shanghai, China) with a three-electrode system.

The gas sensing performance of the prepared In_2O_3 /PANI nanofibers was measured using a custom-built static state gas sensing test system at room temperature ($25 \pm 1\text{ }^\circ\text{C}$) with a relative humidity of $60 \pm 1\%$. During the gas measurement, the aqueous ammonia was injected into the test chamber using a syringe through a rubber plug. The volume of ammonia injected

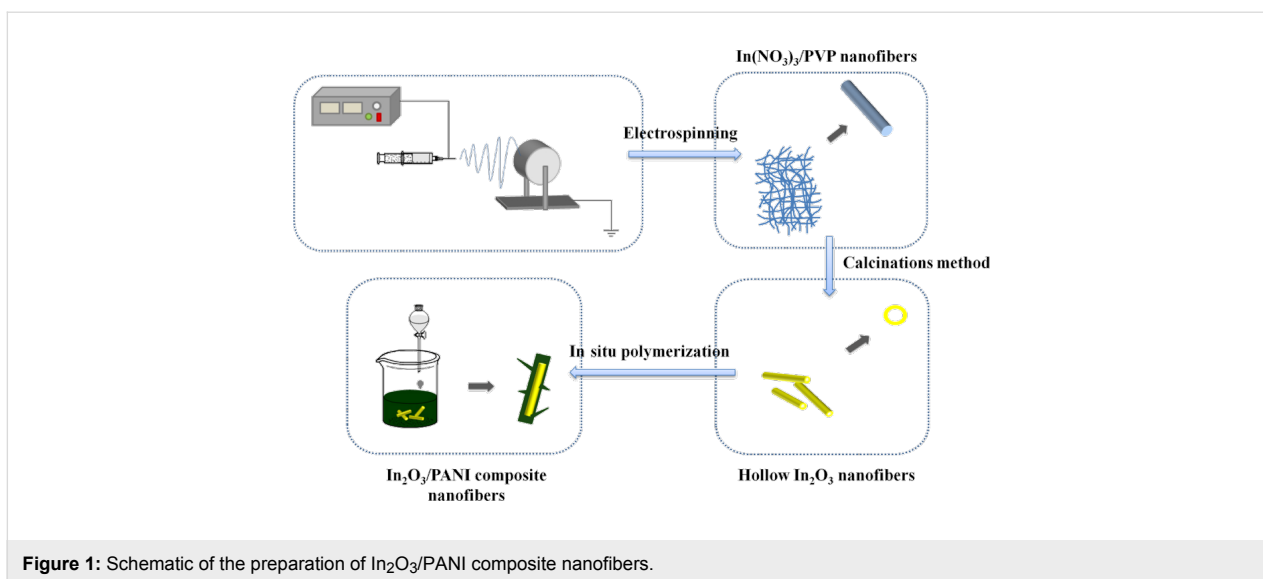


Figure 1: Schematic of the preparation of In₂O₃/PANI composite nanofibers.

into chamber were 1.3468 μL , 4.0404 μL , 6.734 μL , 10.7744 μL and 13.468 μL resulting in ammonia vapor with concentrations of 100, 300, 500, 800 and 1000 ppm, respectively. The gas response value (S) is defined as a ratio of $(R_i - R_0)/R_0$, in which R_i and R_0 are the resistance of the sensor in testing gas and air, respectively. Each result was the average value of five tests.

Results and Discussion

Materials characterization

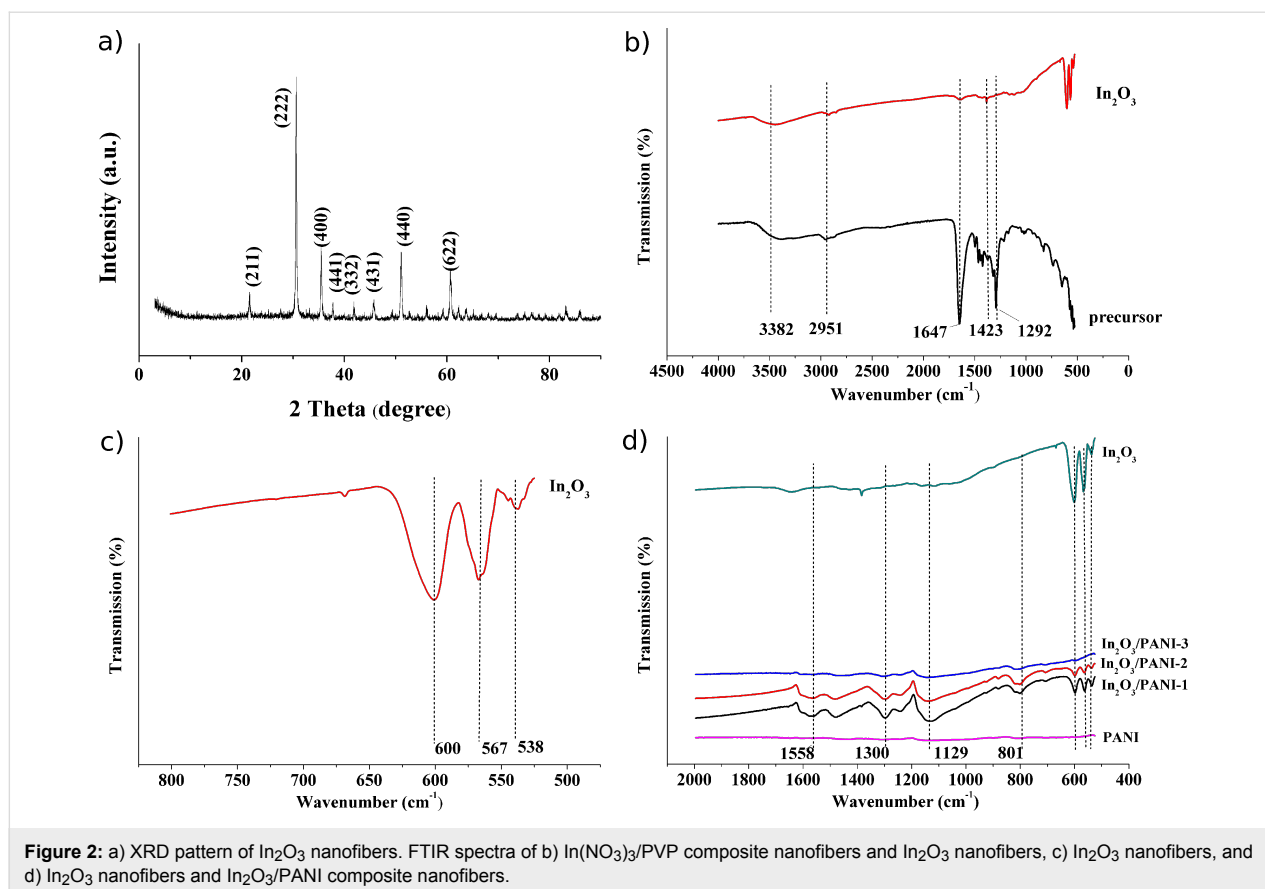
The XRD patterns of the nanofibers obtained by annealing In(NO₃)₃/PVP composite nanofibers at 800 °C are shown in Figure 2a. It can be seen that the crystal phase of the material was In₂O₃, and the diffraction peak of 30.56° was indexed to the (222) crystal plane of the cubic structure of In₂O₃. This result confirmed that the final product of calcination was In₂O₃.

The chemical structure of the precursor nanofibers, In₂O₃ nanofibers and In₂O₃/PANI nanofibers were analyzed by FTIR. As shown in Figure 2b, the FTIR spectrum of In(NO₃)₃/PVP composite nanofibers exhibits a broad characteristic band around 3382 cm^{-1} , which is related to the O–H stretching vibration. It could be the result of absorbing moisture from air. The –CH₂ stretching vibration and bending vibration of PVP are attributed to the peaks of around 2951 cm^{-1} and 1423 cm^{-1} . The peaks at 1647 cm^{-1} and 1292 cm^{-1} were assigned to the C=O stretching vibration and C≡N antisymmetrical stretching vibration, respectively, in the ring skeleton of PVP. But the characteristic peaks of In(NO₃)₃ could not be found in the FTIR spectra. In the spectrum of In₂O₃ nanofibers (Figure 2c), the characteristic peaks of PVP have almost vanished. Instead, peaks around 600 cm^{-1} , 567 cm^{-1} and 538 cm^{-1} appeared, which are

associated with the cubic bixbyite-type structure of In₂O₃. The results indicate that PVP was resolved and In(NO₃)₃ was converted into In₂O₃ during annealing.

Figure 2d presents the FTIR spectra of In₂O₃, PANI and In₂O₃/PANI nanofibers. The characteristic peaks around 1558 cm^{-1} originating from C=C stretching vibration in the quinoid ring of PANI can be seen. The characteristic bands of 1300 cm^{-1} and 1116 cm^{-1} were attributed to the C–N stretching vibration in the benzenoid ring and the bending vibration plane of C–H bonds in the quinoid ring, respectively. By comparison, the characteristic peaks of In₂O₃ also exist in the spectrum of In₂O₃/PANI nanofibers. This demonstrated that PANI was coated on the surface of the In₂O₃ nanofibers by in situ polymerization. But for In₂O₃/PANI-3 nanofibers, the peaks of In₂O₃ and PANI showed a significantly decrease which may be caused by the excess of PANI covering.

Figure 3a,b shows SEM images of In(NO₃)₃/PVP composite nanofibers and In₂O₃ nanofibers, respectively. From Figure 3a, it can be seen that the surface of In(NO₃)₃/PVP composite nanofibers was relatively smooth and no beads and droplets appeared. The diameter distribution of In(NO₃)₃/PVP nanofibers were mostly in the range of 700–1000 nm. The In₂O₃ nanofibers were relatively uniform with diameters of 150–220 nm. These results show that the In₂O₃ nanofibers were much rougher and smaller than the precursor nanofibers. In addition, it shows that some nanofibers adhered together in Figure 3b, which is not the case in Figure 3a. It is possible that the solvent was not completely volatilized from the precursor nanofibers membrane. The residual solvent may have re-dissolved the precursor nanofibers and then the dissolved nanofibers were connected along each other during the calcinations.



As the calcination temperature increased, the residual solvent started to volatilize and the In_2O_3 nanofibers were gradually formed, but the bonded nanofibers would not segregate during this process, leading to some nanofibers connected along each other.

The cross-sectional image and the TEM image show the detailed structure of In_2O_3 nanofibers. In Figure 3c and 3d, it is confirmed that the In_2O_3 nanofibers consisted of small grains and the hollow structure can be clearly observed. The hollow structure of In_2O_3 nanofibers was synthesized by a template-assisted method. PVP as the supporting material of precursor nanofibers was decomposed during the annealing process, and the $\text{In}(\text{NO}_3)_3$ was transformed into crystalline In_2O_3 . During calcination, PVP decomposed and gases diffused from the interior to the exterior of the composite nanofibers, leading to crystalline In_2O_3 grains constantly moving and tending to be regularly arrayed [16]. As a result, hollow structure of In_2O_3 nanofibers was formed during the annealing process.

Current–voltage (I – V) measurements of PANI, $\text{In}_2\text{O}_3/\text{PANI}$ -1, $\text{In}_2\text{O}_3/\text{PANI}$ -2 and $\text{In}_2\text{O}_3/\text{PANI}$ -3 nanofibers were carried out at room temperature. As shown in Figure 4, the I – V characteristics of all $\text{In}_2\text{O}_3/\text{PANI}$ nanofibers clearly exhibit a nonlinear be-

havior and it can be observed the rectifying behavior in Figure 4, which might result from the p–n junction between the p-type PANI and n-type In_2O_3 [28,29]. It can be observed that the current of $\text{In}_2\text{O}_3/\text{PANI}$ showed exponential rise at low voltage and then almost linear rise at high voltages. But for pure PANI, the current showed nearly linear behavior in the forward region, which is attributed to rapidly forming polarons and bipolarons in PANI. As some researches mentioned [28–30], the ohmic behavior in this case was related to the formation of an ohmic contact between PANI and In_2O_3 . Compared with pure PANI, the $\text{In}_2\text{O}_3/\text{PANI}$ nanofibers reach a higher current due to the smaller width of the depletion layer between PANI and In_2O_3 . Moreover, the addition of PANI reduced the width of the depletion layer at the interface and was helpful to form a typical ohmic system [31]. Thus, it can be confirmed that a p–n junction between PANI and In_2O_3 had been formed.

Gas sensing properties

To study the ammonia sensing behavior of the sensors with different ratios of In_2O_3 to aniline, the dynamic response of the sensors based on pure PANI and $\text{In}_2\text{O}_3/\text{PANI}$ nanofibers towards different NH_3 concentrations ranging from 100 to 1000 ppm at room temperature were investigated. As exhibited in Figure 5, it can be seen that the trends of the response and

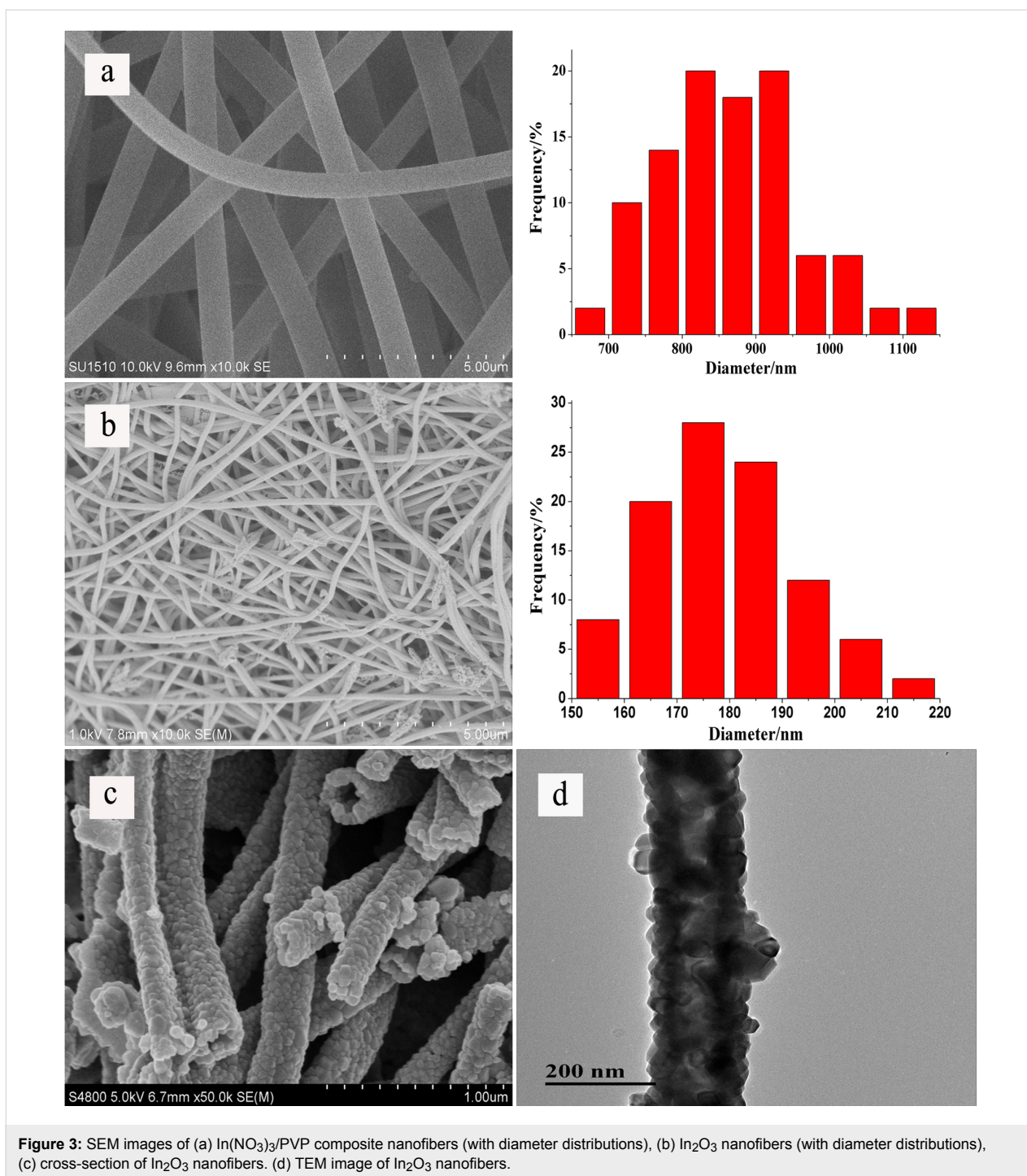


Figure 3: SEM images of (a) In(NO₃)₃/PVP composite nanofibers (with diameter distributions), (b) In₂O₃ nanofibers (with diameter distributions), (c) cross-section of In₂O₃ nanofibers. (d) TEM image of In₂O₃ nanofibers.

recovery were consistent among the pure PANI and the three In₂O₃/PANI nanofibers sensors. The In₂O₃/PANI-1 and In₂O₃/PANI-2 nanofibers always show a higher response value than pure PANI at the same concentration of NH₃.

The response values of pure PANI and these three In₂O₃/PANI nanofibers sensors to different concentrations of NH₃ are displayed in Figure 6. It can be found that the response values

increased with the growth of gas concentration. The responses of pure PANI to 100 ppm, 300 ppm, 500 ppm, 800 ppm, 1000 ppm NH₃ were 1.26, 3.11, 5.91, 7.71, 10.09, respectively. The responses of In₂O₃/PANI-1 nanofibers sensor were 1.48, 5.32, 14.11, 16.00 and 21.12. For In₂O₃/PANI-2 nanofibers sensor, the responses were 1.48, 5.48, 17.67, 36.57 and 53.20, respectively. While for the In₂O₃/PANI-3 sensor, the values were only 0.76, 3.32, 4.64, 11.15 and 14.43. It was observed

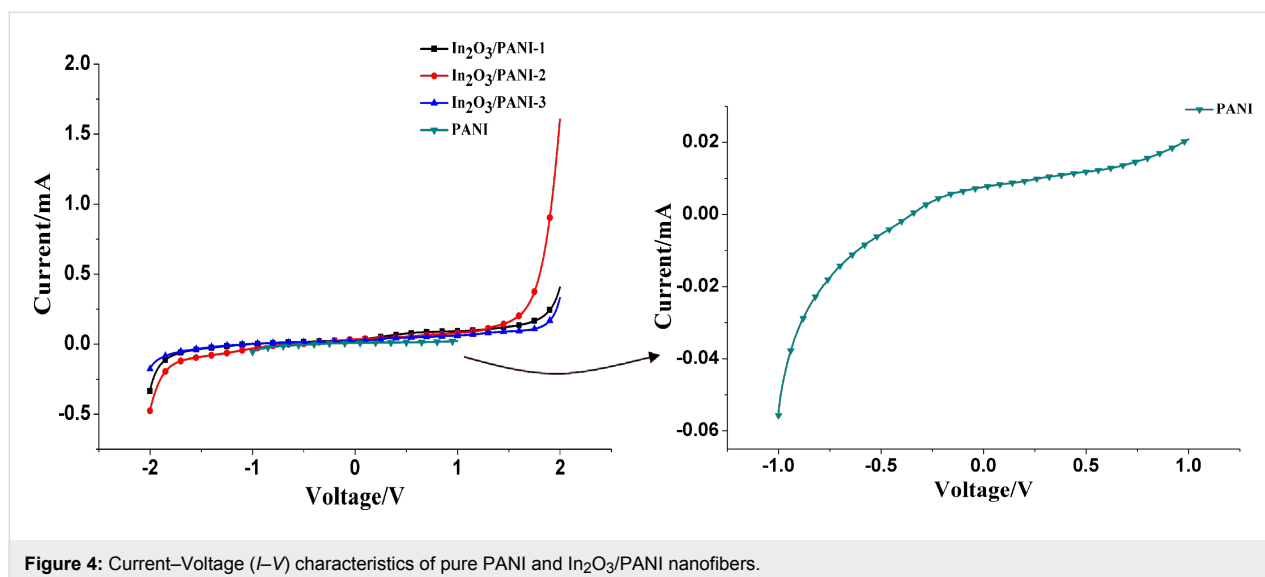


Figure 4: Current–Voltage (I – V) characteristics of pure PANI and $\text{In}_2\text{O}_3/\text{PANI}$ nanofibers.

that at low concentrations of NH_3 , the responses of these sensors were similar. But with increasing NH_3 concentrations, it was very clear that the responses of $\text{In}_2\text{O}_3/\text{PANI}$ gas sensors were much higher than pure PANI. The response of $\text{In}_2\text{O}_3/\text{PANI-2}$ exhibited the highest value. The response of $\text{In}_2\text{O}_3/\text{PANI-2}$ to 1000 ppm was about twice as large as that of $\text{In}_2\text{O}_3/\text{PANI-1}$. When the weight ratio of In_2O_3 to aniline was raised to 1:4 ($\text{In}_2\text{O}_3/\text{PANI-3}$), the responses to NH_3 decreased.

These results revealed that the mass ratio of In_2O_3 to aniline had an obvious influence on the NH_3 sensing performance of the composite nanofibers. Comparing the sensitivity of three $\text{In}_2\text{O}_3/\text{PANI}$ nanofibers sensors, it can be found that the $\text{In}_2\text{O}_3/\text{PANI-2}$ nanofibers sensor delivers the best performance. Therefore, $\text{In}_2\text{O}_3/\text{PANI-2}$ was selected to further investigate the sensing properties.

As mentioned in the Introduction section, 50 ppm NH_3 will cause harm to human health. Accordingly, the response of the $\text{In}_2\text{O}_3/\text{PANI-2}$ sensor to 50 ppm, 30 ppm and 10 ppm were investigated. As shown in Figure 7, the response of the $\text{In}_2\text{O}_3/\text{PANI-2}$ sensor to low concentration (10–50 ppm) NH_3 was 0.12, 0.48 and 0.94, respectively. Thus it can be seen the $\text{In}_2\text{O}_3/\text{PANI-2}$ sensor had good response performance towards low concentrations of NH_3 .

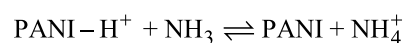
The cross-response test was used to evaluate the selectivity of $\text{In}_2\text{O}_3/\text{PANI-2}$ nanofibers sensor. Figure 8 shows the dynamic response of $\text{In}_2\text{O}_3/\text{PANI-2}$ nanofibers sensor to methanol, ethanol, acetone and ammonia at a concentration of 1000 ppm. It is obvious that the $\text{In}_2\text{O}_3/\text{PANI-2}$ nanofibers sensor was almost insensitive to methanol, ethanol and acetone vapors. According to the test results, it can be concluded that $\text{In}_2\text{O}_3/\text{PANI-2}$

nanofibers sensor exhibited unique selectivity to ammonia. A possible mechanism for the selectivity to NH_3 is the chemisorption of NH_3 on PANI in $\text{In}_2\text{O}_3/\text{PANI-2}$ forming ammonium [32]. Besides, the different gases show different electron affinity values [33], and the varying sensitivity of $\text{In}_2\text{O}_3/\text{PANI-2}$ nanofibers to different gases may be explained by this.

$\text{In}_2\text{O}_3/\text{PANI-2}$ nanofibers sensor was exposed to 1000 ppm ammonia for five times to investigate the repeatability and reversibility. As shown in Figure 9, the recovery of the $\text{In}_2\text{O}_3/\text{PANI-2}$ nanofibers sensor could not fully return to the initial state, and there was a baseline drift of 4% after the first exposure to NH_3 . This bias was smaller than the results in other reports [34–36]. On the other hand, the response of this sensor slightly decreased with the increasing number of tests. The final response reached 47.42, which was about 89% of the first test. Hence, the $\text{In}_2\text{O}_3/\text{PANI-2}$ nanofibers sensor showed good repeatability and reversibility.

Gas sensing mechanism

It is well known that the chemical sensors are composed of two parts, an active part and a transduction part, whose function is sensitive to gas analytes and produces a signal that is related to the concentration [19]. In this study, PANI acted as an active element which can react with NH_3 resulting in the transformation of PANI from emeraldine salt to emeraldine base by dedoping. The reaction between PANI and NH_3 can be described as follows:



The absorption of NH_3 caused the deprotonation of the N-H^+ site of the emeraldine salt, leading to a significantly increased

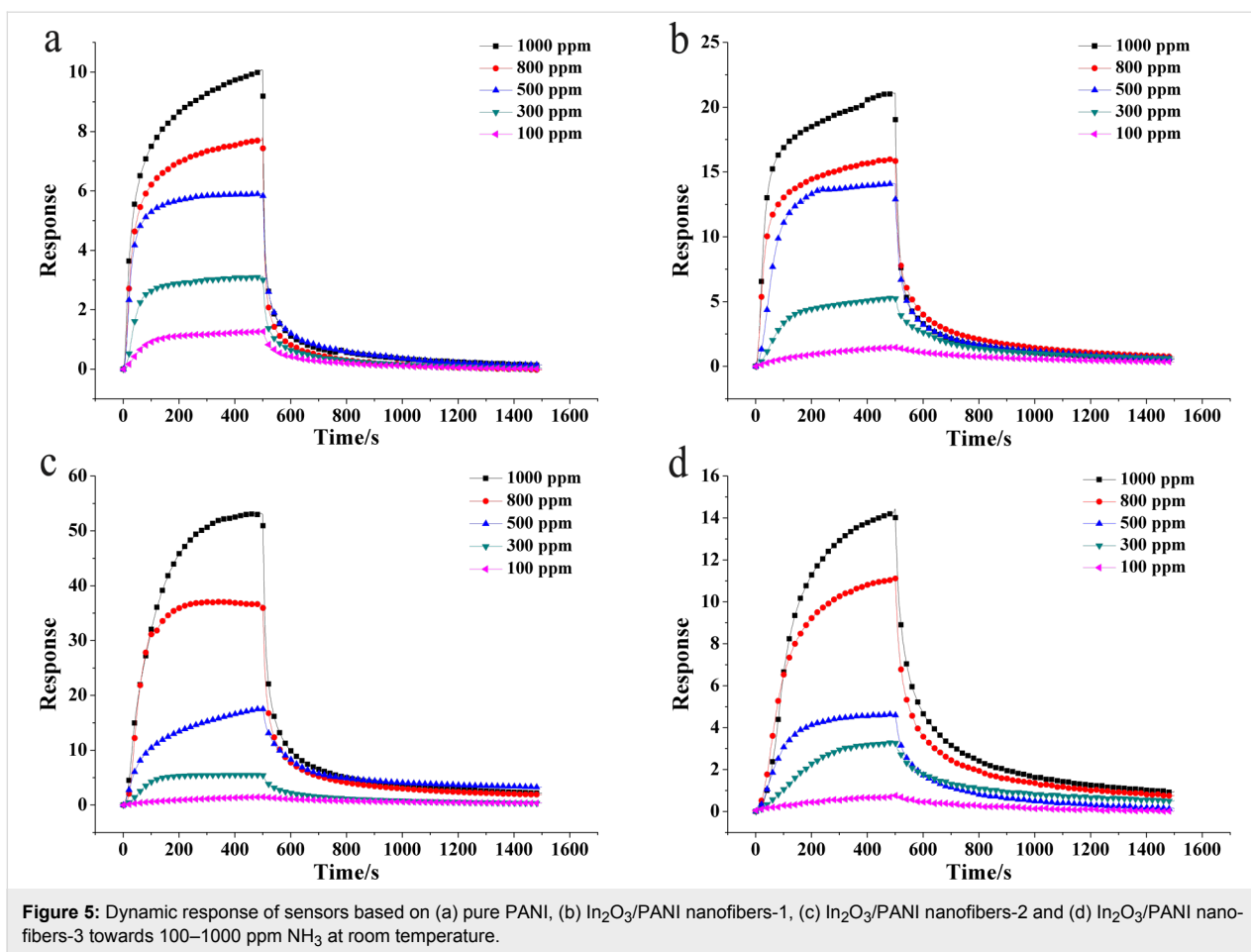


Figure 5: Dynamic response of sensors based on (a) pure PANI, (b) $\text{In}_2\text{O}_3/\text{PANI}$ nanofibers-1, (c) $\text{In}_2\text{O}_3/\text{PANI}$ nanofibers-2 and (d) $\text{In}_2\text{O}_3/\text{PANI}$ nanofibers-3 towards 100–1000 ppm NH_3 at room temperature.

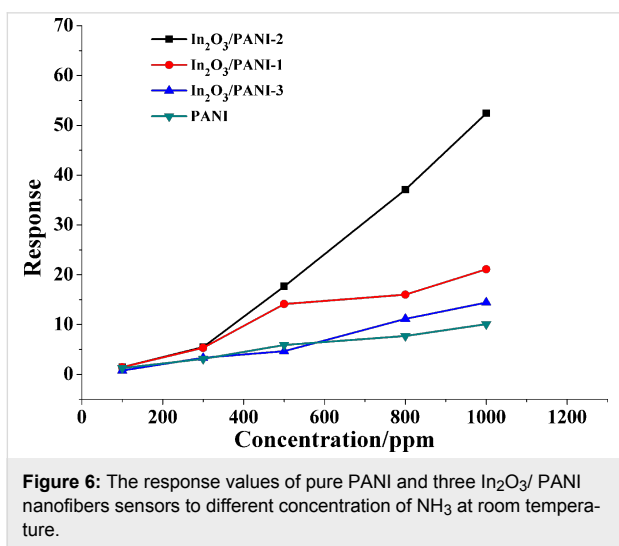


Figure 6: The response values of pure PANI and three $\text{In}_2\text{O}_3/\text{PANI}$ nanofibers sensors to different concentration of NH_3 at room temperature.

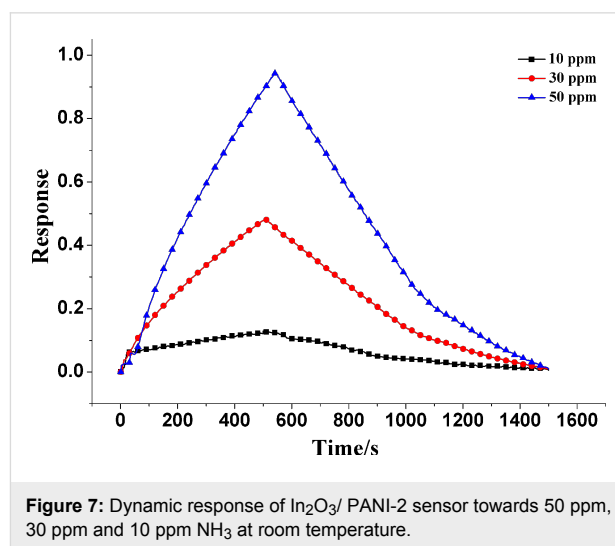


Figure 7: Dynamic response of $\text{In}_2\text{O}_3/\text{PANI}$ -2 sensor towards 50 ppm, 30 ppm and 10 ppm NH_3 at room temperature.

resistance [37,38]. When this reaction reached equilibrium in NH_3 atmosphere, the resistance of the PANI-based sensor maintained a constant value. When the sensor was exposed to air, NH_3 is volatilized and the resistance of the PANI composite nanofibers is reduced. Therefore, due to the unique mechanism,

PANI (emeraldine salt) based sensors exhibited a great selectivity to NH_3 .

As the $I-V$ characteristics show, it is confirmed that p–n heterojunctions had been formed between PANI and In_2O_3 nano-

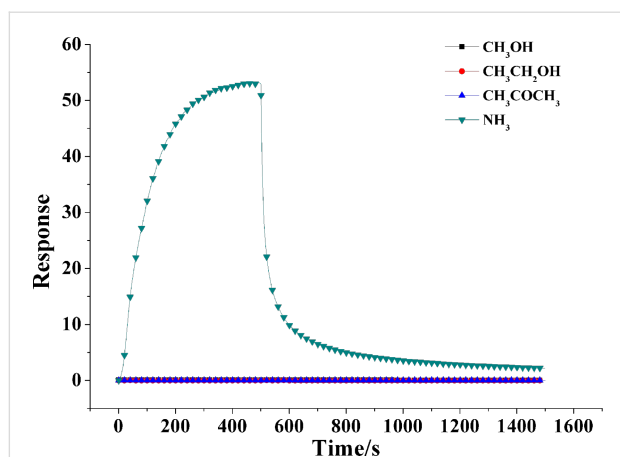


Figure 8: Cross-response curves of $\text{In}_2\text{O}_3/\text{PANI-2}$ nanofibers sensor to 1000 ppm methanol, ethanol, acetone and ammonia.

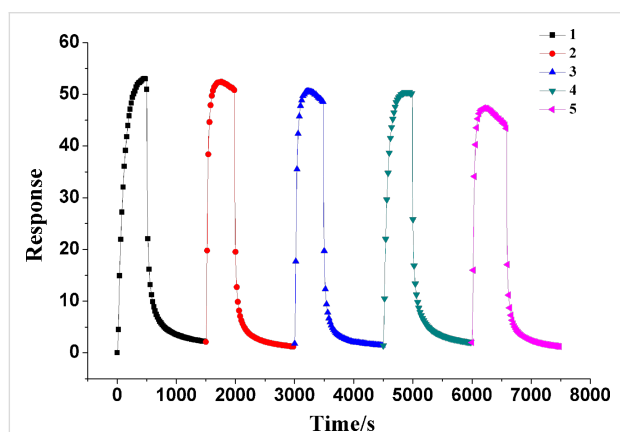


Figure 9: Sensing repeatability and reversibility of $\text{In}_2\text{O}_3/\text{PANI-2}$ nanofibers sensor to 1000 ppm NH_3 vapor.

fibers, in which PANI is a p-type semiconductor and In_2O_3 nanofibers presents as an n-type semiconductor [21,27,34]. The changes of the depletion layer of the p–n heterojunction are shown in Figure 10. The width of the depletion section is related to the doping concentration [39]. With low concentration doping, it needs a sufficiently thick depletion layer to provide impurity atoms to build an internal field. Accordingly, on exposure to NH_3 , the protons from PANI are transferred to the NH_3 molecules, which results in a widening of the depletion layer in the PANI section [40]. Simultaneously, the variation of the PANI region width would have effects on the width of the In_2O_3 region and on the p–n junction. The electrons of In_2O_3 and holes of PANI move in opposite directions until the new Fermi level ($E_{F-\text{NH}_3}$) reaches equilibrium. In this process, the electron transfer between the n-type In_2O_3 and p-type PANI is obstructed due to the potential barrier. Thus the depletion layer between PANI and In_2O_3 becomes wider and the resistance of the material increases [27,41,42]. According to the

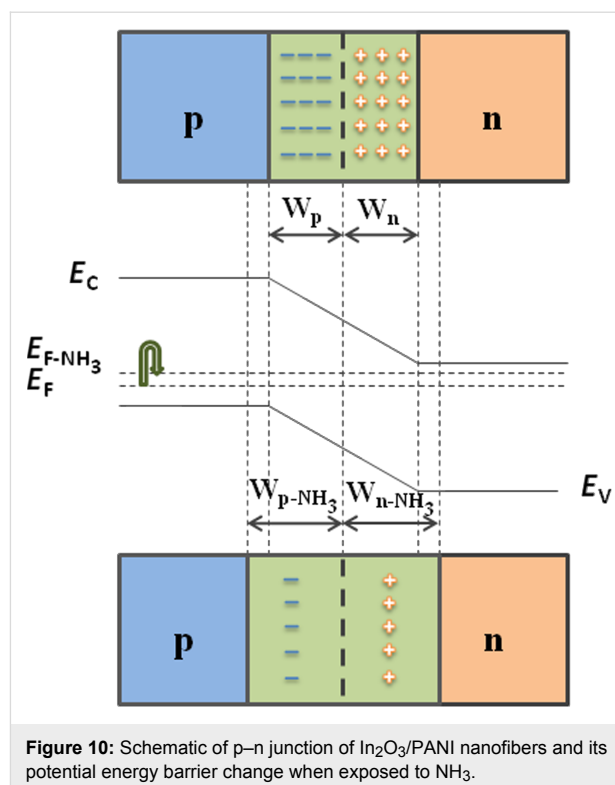


Figure 10: Schematic of p–n junction of $\text{In}_2\text{O}_3/\text{PANI}$ nanofibers and its potential energy barrier change when exposed to NH_3 .

response definition ($S = (R_1 - R_0)/R_0$), the increase in resistance attributed to the p–n junction increases the sensitivity of composite nanofibers sensors. In addition, the sensitivity of the composite gas sensor materials is also connected to the mass ratio of In_2O_3 and aniline.

Because of the smaller amount of polyaniline, which acts as active material in this composite system, the $\text{In}_2\text{O}_3/\text{PANI-1}$ gas sensor showed a lower sensitivity. However, for the $\text{In}_2\text{O}_3/\text{PANI-3}$ gas sensor, the external surface of In_2O_3 nanofibers was coated with excess polyaniline, yielding a gas sensing performance similar to that of pure PANI. Even the response of $\text{In}_2\text{O}_3/\text{PANI-3}$ to 100 ppm and 500 ppm NH_3 was less than that of pure PANI. The p–n junction of In_2O_3 and PANI in $\text{In}_2\text{O}_3/\text{PANI-3}$ does not work efficiently. In general, the characteristic of the gas sensitive material response was discrete instead of ideally linear [34,36,43]. For $\text{In}_2\text{O}_3/\text{PANI-3}$ and pure PANI, the characteristic responses were similar. Therefore, it was possible that the response of $\text{In}_2\text{O}_3/\text{PANI-3}$ were less than that of pure PANI, especially towards lower concentrations of NH_3 . In this study, when the mass ratio of In_2O_3 to aniline was 1:2, the gas sensor material exhibited optimum performance in detecting NH_3 .

Conclusion

$\text{In}_2\text{O}_3/\text{PANI}$ nanofibers with reliable sensing properties towards NH_3 were synthesized by electrospinning, calcination and in

situ polymerization. The gas sensors based on In₂O₃/PANI nanofibers exhibited a higher sensitivity than pure PANI. The In₂O₃/PANI-2 nanofiber sensor exhibited the best sensitivity to NH₃ vapor at room temperature, and this sensor was further investigated for its selectivity by interfering with methanol, ethanol and acetone vapors. The results indicated that the In₂O₃/PANI-2 nanofiber sensor had excellent selectivity, good repeatability and reversibility. The enhancement of gas sensing performance of In₂O₃/PANI nanofiber sensor may be attributed to formation of a p–n junction between In₂O₃ and PANI, which existence is confirmed by the *I–V* characteristics.

References

- Tang, Y.-L.; Li, Z.-J.; Ma, J.-Y.; Su, H.-Q.; Guo, Y.-J.; Wang, L.; Du, B.; Chen, J.-J.; Zhou, W.; Yu, Q.-K.; Zu, X.-T. *J. Hazard. Mater.* **2014**, *280*, 127–133. doi:10.1016/j.jhazmat.2014.08.001
- Wu, Z.; Chen, X.; Zhu, S.; Zhou, Z.; Yao, Y.; Quan, W.; Liu, B. *Sens. Actuators, B* **2013**, *178*, 485–493. doi:10.1016/j.snb.2013.01.014
- Na, K.; Song, C.; Switzer, C.; Cocker, D. R., III. *Environ. Sci. Technol.* **2007**, *41*, 6096–6102. doi:10.1021/es061956y
- Jabłońska, M.; Palkovits, R. *Appl. Catal., B* **2016**, *181*, 332–351. doi:10.1016/j.apcatb.2015.07.017
- Swotinsky, R. B.; Chase, K. H. *Am. J. Ind. Med.* **1990**, *17*, 515–521. doi:10.1002/ajim.4700170409
- Park, S.-J.; Jin, S.-Y. *J. Colloid Interface Sci.* **2005**, *286*, 417–419. doi:10.1016/j.jcis.2005.01.043
- Yoo, K.-P.; Kwon, K.-H.; Mi, N.-K.; Lee, M. J.; Lee, C. J. *Sens. Actuators, B* **2009**, *143*, 333–340. doi:10.1016/j.snb.2009.09.029
- Li, C.; Zhang, D.; Lei, B.; Han, S.; Liu, X.; Zhou, C. *J. Phys. Chem. B* **2003**, *107*, 12451–12455. doi:10.1021/jp0361531
- Biskupski, D.; Herbig, B.; Schottner, G.; Moos, R. *Sens. Actuators, B* **2011**, *153*, 329–334. doi:10.1016/j.snb.2010.10.029
- Shahabuddin, M.; Sharma, A.; Kumar, J.; Tomar, M.; Umar, A.; Gupta, V. *Sens. Actuators, B* **2014**, *194*, 410–418. doi:10.1016/j.snb.2013.12.097
- Renganathan, B.; Sastikumar, D.; Gobi, G.; Yogamalar, N. R.; Bose, A. C. *Opt. Laser Technol.* **2011**, *43*, 1398–1404. doi:10.1016/j.optlastec.2011.04.008
- Nguyen, D. D.; Dang, D. V.; Nguyen, D. C. *Adv. Nat. Sci.: Nanosci. Nanotechnol.* **2015**, *6*, 035006. doi:10.1088/2043-6262/6/3/035006
- Zhang, D.; Liu, Z.; Li, C.; Tang, T.; Liu, X.; Han, S.; Lei, B.; Zhou, C. *Nano Lett.* **2004**, *4*, 1919–1924. doi:10.1021/nl0489283
- Miller, D. R.; Akbar, S. A.; Morris, P. A. *Sens. Actuators, B* **2014**, *204*, 250–272. doi:10.1016/j.snb.2014.07.074
- Zhan, Z.; Jiang, D.; Xu, J. *Mater. Chem. Phys.* **2005**, *90*, 250–254. doi:10.1016/j.matchemphys.2004.01.043
- Liang, X.; Jin, G.; Liu, F.; Zhang, X.; An, S.; Ma, J.; Lu, G. *Ceram. Int.* **2015**, *41*, 13780–13787. doi:10.1016/j.ceramint.2015.08.060
- Li, Z.; Fan, Y.; Zhan, J. *Eur. J. Inorg. Chem.* **2010**, *2010*, 3348–3353. doi:10.1002/ejic.201000313
- Li, H.; Liu, Y.; Luo, L.; Tan, Y.; Zhang, Q.; Li, K. *Mater. Sci. Eng., C* **2016**, *59*, 438–444. doi:10.1016/j.msec.2015.10.036
- Fratoddi, I.; Venditti, I.; Cametti, C.; Russo, M. V. *Sens. Actuators, B* **2015**, *220*, 534–548. doi:10.1016/j.snb.2015.05.107
- Lakard, B.; Carquigny, S.; Segut, O.; Patios, T.; Lakard, S. *Metals (Basel, Switz.)* **2015**, *5*, 1371–1386. doi:10.3390/met5031371
- Gong, J.; Li, Y.; Hu, Z.; Zhou, Z.; Deng, Y. *J. Phys. Chem. C* **2010**, *114*, 9970–9974. doi:10.1021/jp100685r
- Timmer, B.; Olthuis, W.; van den Berg, A. *Sens. Actuators, B* **2005**, *107*, 666–677. doi:10.1016/j.snb.2004.11.054
- Pawar, S. G.; Chougule, M. A.; Patil, S. L.; Raut, B. T.; Godse, P. R.; Sen, S.; Patil, V. B. *IEEE Sens. J.* **2011**, *11*, 3417–3423. doi:10.1109/JSEN.2011.2160392
- Nasirian, S.; Milani, M. H. *Appl. Surf. Sci.* **2015**, *328*, 395–404. doi:10.1016/j.apsusc.2014.12.051
- Sadek, A. Z.; Wlodarski, W.; Shin, K.; Kaner, R. B.; Kalantar-zadeh, K. *Synth. Met.* **2008**, *158*, 29–32. doi:10.1016/j.synthmet.2007.11.008
- Betty, C. A.; Choudhury, S.; Arora, S. *Sens. Actuators, B* **2015**, *220*, 288–294. doi:10.1016/j.snb.2015.05.074
- Pang, Z.; Fu, J.; Luo, L.; Huang, F.; Wei, Q. *Colloids Surf., A* **2014**, *461*, 113–118. doi:10.1016/j.colsurfa.2014.07.038
- Abaci, S.; Nessark, B.; Riahi, F. *Ionics* **2014**, *20*, 1693–1702. doi:10.1007/s11581-014-1129-9
- Ameen, S.; Shaheer, A. M.; Ansari, S. G.; Yang, O.-B.; Shin, H.-S. *Superlattices Microstruct.* **2009**, *46*, 872–880. doi:10.1016/j.spmi.2009.09.007
- Li, Y.; Gong, J.; McCune, M.; He, G.; Deng, Y. *Synth. Met.* **2010**, *160*, 499–503. doi:10.1016/j.synthmet.2009.11.037
- Pandey, S. S.; Rikitake, K.; Takashima, W.; Kaneto, K. *Curr. Appl. Phys.* **2003**, *3*, 107–113. doi:10.1016/S1567-1739(02)00179-7
- Tai, H.; Xu, X.; Ye, Z.; Liu, C.; Xie, G.; Jiang, Y. *Chem. Phys. Lett.* **2015**, *621*, 58–64. doi:10.1016/j.cplett.2014.12.052
- Pawar, S. G.; Chougule, M. A.; Shashwati, S.; Patil, V. B. *J. Appl. Polym. Sci.* **2012**, *125*, 1418–1424. doi:10.1002/app.35468
- Wang, L.; Huang, H.; Xiao, S.; Cai, D.; Liu, Y.; Liu, B.; Wang, D.; Wang, C.; Li, H.; Wang, Y.; Li, Q.; Wang, T. *ACS Appl. Mater. Interfaces* **2014**, *6*, 14131–14140. doi:10.1021/am503286h
- Matsuguchi, M.; Asahi, T. *Sens. Actuators, B* **2011**, *160*, 999–1004. doi:10.1016/j.snb.2011.09.017
- Joulazadeh, M.; Navarchian, A. H. *Synth. Met.* **2015**, *210*, 404–411. doi:10.1016/j.synthmet.2015.10.026
- Zhang, Y.; Kim, J. J.; Chen, D.; Tuller, L. H.; Rutledge, C. C. *Adv. Funct. Mater.* **2014**, *24*, 4005–4014. doi:10.1002/adfm.201400185
- Srinives, S.; Sarkar, T.; Mulchandani, A. *Electroanalysis* **2013**, *25*, 1439–1445. doi:10.1002/elan.201300015
- Mane, A. T.; Navale, S. T.; Patil, V. B. *Org. Electron.* **2015**, *19*, 15–25. doi:10.1016/j.orgel.2015.01.018
- Bai, S.; Tian, Y.; Cui, M.; Sun, J.; Tian, Y.; Luo, R.; Chen, A.; Li, D. *Sens. Actuators, B* **2016**, *226*, 540–547. doi:10.1016/j.snb.2015.12.007
- Xu, H.; Ju, D.; Li, W.; Gong, H.; Zhang, J.; Wang, J.; Cao, B. *Sens. Actuators, B* **2016**, *224*, 654–660. doi:10.1016/j.snb.2015.10.076
- Bai, S.; Ma, Y.; Luo, R.; Chen, A.; Li, D. *RSC Adv.* **2016**, *6*, 2687–2694. doi:10.1039/C5RA20843B
- Li, Y.; Ban, H.; Yang, M. *Sens. Actuators, B* **2016**, *224*, 449–457. doi:10.1016/j.snb.2015.10.078

License and Terms

This is an Open Access article under the terms of the Creative Commons Attribution License (<http://creativecommons.org/licenses/by/4.0>), which permits unrestricted use, distribution, and reproduction in any medium, provided the original work is properly cited.

The license is subject to the *Beilstein Journal of Nanotechnology* terms and conditions: (<http://www.beilstein-journals.org/bjnano>)

The definitive version of this article is the electronic one which can be found at:
[doi:10.3762/bjnano.7.122](https://doi.org/10.3762/bjnano.7.122)